Excitations and dynamical structure factor of J_1-J_2 spin-$\frac{3}{2}$ and spin-$\frac{5}{2}$ Heisenberg spin chains

Aman Sharma [1,*] Mithilesh Nayak [2,3] Natalia Chepiga [4] and Frédéric Mila [1]

[1]*Institute of Physics, École Polytechnique Fédérale de Lausanne (EPFL), Lausanne, Switzerland*

[2]*Department of Physics, University of Fribourg, 1700 Fribourg, Switzerland*

[3]*Department of Physics and Astronomy, The University of Tennessee, Knoxville, Tennessee 37996, USA*

[4]*Kavli Institute of Nanoscience, Delft University of Technology, Lorentzweg 1, 2628 CJ Delft, The Netherlands*

(Received 19 June 2025; revised 11 August 2025; accepted 15 August 2025; published 2 September 2025)

We study the dynamical structure factor of the frustrated spin-3/2 J_1-J_2 Heisenberg chains, with particular focus on the partially dimerized phase that emerges between two Kosterlitz-Thouless transitions. Using a valence bond solid *Ansatz* corroborated by density-matrix renormalization-group simulations, we investigate the nature of magnon and spinon excitations through the single-mode approximation. We show that the magnon develops an incommensurate dispersion at $J_2 \approx 0.32J_1$, while the spinons, viewed as domain walls between degenerate valence bond solid states, become incommensurate at $J_2 \approx 0.4J_1$ beyond the Lifshitz point ($J_2 \approx 0.388J_1$). The dynamical structure factor exhibits rich spectral features shaped by the interplay between these excitations, with magnons appearing as resonances embedded in the spinon continuum. The spinon gap shows a nonmonotonic behavior, reaching a peak near the center of the partially dimerized phase and closing at the boundaries, suggesting the appearance of a floating phase as a result of the condensation of incommensurate spinons. Comparative analysis with the spin-5/2 case confirms the universality of these phenomena across half-integer higher-spin systems. Our results provide detailed insight into how fractionalization and incommensurate condensation govern the spectral properties of frustrated spin chains, offering a unified picture across different spin magnitudes.

DOI: 10.1103/pddz-42x9

I. INTRODUCTION

Quantum spin chains serve as fundamental models for studying strongly correlated systems and have been instrumental in revealing novel phases of matter, quantum criticality, and exotic excitations [1,2]. Among the simplest and most thoroughly explored is the J_1-J_2 Heisenberg chain with spin-1/2, which has provided deep insight into the role of frustration in one-dimensional systems [3,4]. The model is defined by the Hamiltonian:

$$H = J_1 \sum_{i=1}^{N} \mathbf{S}_i \cdot \mathbf{S}_{i+1} + J_2 \sum_{i=1}^{N} \mathbf{S}_i \cdot \mathbf{S}_{i+2}, \qquad (1)$$

where J_1 and J_2 are antiferromagnetic interactions between nearest and next-nearest neighbors, respectively. This model exhibits a rich phase diagram due to the competition between nearest-neighbor (J_1) and next-nearest-neighbor (J_2) antiferromagnetic interactions. At small J_2, the system remains gapless and critical, described by the $SU(2)_1$ Wess-Zumino-Witten (WZW) conformal field theory [5–7]. As J_2 increases beyond $J_2 \approx 0.2411J_1$ [4], the system undergoes a Berezinskii-Kosterlitz-Thouless (BKT) transition into a gapped dimerized phase with spontaneously broken translation symmetry and short-range correlations [8,9]. The excitations in this regime fractionalize into spinons, and the spectrum becomes incommensurate for large enough J_2, signaling a Lifshitz transition [10–12].

The spin-1 J_1-J_2 chain exhibits a qualitatively different behavior [13]. At $J_2 = 0$, the system lies in the celebrated Haldane phase, a gapped phase with hidden topological order and exponentially decaying correlations [14–16]. As J_2 increases, the system remains gapped, but at a critical value of $J_2 \approx 0.76J_1$, it undergoes a first-order phase transition into a next-nearest-neighbor Haldane phase [17,18]. Remarkably, at the transition point, the lowest excitations are spinons, domain walls that separate regions of Haldane and NNN Haldane order. These spinons are deconfined and exhibit a narrow but incommensurate dispersion. Away from the transition, the spinons become confined into magnon bound states, and the spectrum evolves into that of conventional triplet excitations [19,20].

Motivated by these foundational studies, recent attention has turned to higher-spin models [21,22], where quantum fluctuations are reduced but frustration remains potent. In this regard, the spin-3/2 J_1-J_2 Heisenberg chain presents a particularly intriguing case due to its intermediate position between half-integer and higher-spin behaviors [21,23]. Quantum fluctuations are still significant, yet the Hilbert space is rich enough to support complex valence bond structures. The model has garnered interest due to the interplay of frustration and quantum fluctuations, which gives rise to a rich phase diagram characterized by critical, dimerized, and floating phases [21]. For small values of J_2, the system remains in a critical gapless phase described by the WZW $SU(2)_1$ universality class. However, as J_2 increases, the system undergoes a BKT transition to a partially dimerized gapped phase, where the translation symmetry is spontaneously broken. Upon further

*Contact author: a.sharma@epfl.ch

increasing J_2, another BKT transition closes the spectral gap, leading to a floating phase with incommensurate correlations [21,24]. An outstanding question raised by these studies is the microscopic origin of the reentrant, gapless floating phase first identified numerically for the spin-3/2 chain [21] and later observed also for $S = 5/2$ [22] which came as a surprise. One of the aims of the present work is to provide a qualitative explanation of the emergence of this phase using a variational single-mode analysis of spinons built on VBS states. Finally, at sufficiently large J_2, the system undergoes a transition into a fully dimerized phase, akin to what has been observed in higher-spin systems [22].

While significant efforts have been devoted to understanding the static properties of these phases [21,24], the nature of excitations and their contributions to the dynamical structure factor (DSF) remain less explored. The DSF is a crucial quantity that encodes information about spin dynamics and can be directly probed in inelastic neutron-scattering experiments. Notably, the transition into incommensurate behavior and the interplay between magnon and spinon excitations in the partially dimerized phase raise intriguing questions about the spectral evolution across different regimes. While quantum fluctuations are comparatively weaker in spin-5/2 systems, the phase diagram remains qualitatively similar, exhibiting a partially dimerized phase and transitions into incommensurate regimes [22].

In this work, we investigate the dynamical properties of the partially dimerized phase in the spin-3/2 J_1-J_2 chain. Employing a valence bond solid (VBS) *Ansatz* [25–27], validated against density-matrix renormalization-group (DMRG) calculations [28,29], we analyze the dispersion relations of both magnon and spinon excitations. Using the single-mode approximation (SMA) [30–33], we demonstrate that the magnons develop an incommensurate dispersion at $J_2 \approx 0.32J_1$, whereas spinons become incommensurate at a larger critical value, $J_2 \approx 0.4J_1$. This is consistent with the Lifshitz transition at $J_2 \approx 0.388J_1$, as identified in prior studies [24]. Moreover, we show that the gapless phases surrounding the partially dimerized phase can both be interpreted as the condensation of spinons. Finally, we turn to the spin-5/2 J_1-J_2 Heisenberg chain to examine the robustness of these features in higher-spin settings. Our comparative analysis reveals a consistent pattern in the evolution of magnon and spinon excitations across spin values in half-integer spin chains.

The rest of the paper is structured as follows: In Sec. II, we describe the numerical methods and the construction of spinon and magnon excitations using SMA. Section III presents the DSF results and their comparison with SMA predictions. In Sec. IV, we analyze the evolution of excitation spectra and incommensurability. Section V concludes with a summary and outlook.

II. METHODS

A. Time-dependent density matrix renormalization group

To calculate the DSF of spin-3/2 and spin-5/2 Heisenberg chains with competing J_1 and J_2 interactions, we used the time-dependent density-matrix renormalization-group (tDMRG) method (sometimes also called TEBD, see Ref. [34] for terminology) [28,29,34–37]. The DSF at zero temperature is defined as

$$S^{\alpha\alpha}(k,\omega) = \int dt\, e^{-i\omega t} \sum_{r_i,r_j} e^{ik(r_i-r_j)} \langle\psi_0| S^{\alpha}_{r_i}(t) S^{\alpha}_{r_j} |\psi_0\rangle ,$$

where $\alpha = x, y, z$, and $|\psi_0\rangle$ denotes the ground state. Physically, this DSF represents the Fourier transform of time-dependent spin-spin correlations and can be experimentally measured via inelastic neutron scattering (INS). In this work, since we are interested in a Hamiltonian invariant by rotation in spin space, we only consider the $S^{zz}(k,\omega)$ component of the DSF. In SU(2)-symmetric systems, all spin components are equivalent, so this choice serves as a representative channel.

The calculation of the DSF involves two main computational steps: (i) accurate determination of the ground-state wave function, and (ii) real-time evolution of a state obtained by applying a spin operator to the ground state.

1. Ground-state calculation

The ground states of the spin-3/2 and spin-5/2 Heisenberg chains are computed using the standard DMRG method, employing a matrix product state (MPS) *Ansatz* [34–37]. We considered finite-size chains with 150 sites, using a fixed bond dimension $\chi = 200$–250 in the MPS representation, for spin-3/2. For spin-5/2, we used chains of 90 sites that were simulated with $\chi = 150$. Iterative sweeping with the one-site update algorithm continued until the variance per site reached a threshold of 10^{-3}–10^{-6} for spin-3/2 or 10^{-3}–10^{-5} for spin-5/2, ensuring a moderate to good accuracy of the ground states obtained for all parameter values of interest. Although fixed bond dimension DMRG may, in principle, risk convergence to metastable or locally optimal solutions, we verified the reliability of our ground states by performing additional convergence tests. Specifically, at selected representative points, we repeated calculations with larger bond dimensions and confirmed that the corresponding DSFs remained qualitatively and quantitatively unchanged (see Appendix B).

Our implementation is capable of handling much larger bond dimensions than those used in this study, allowing for high accuracy. However, larger bond dimensions significantly slow the real-time evolution in tDMRG simulations, thereby significantly increasing the computational cost. As a result, we chose to work with moderately sized systems. In our simulations, we fix the bond dimension χ throughout the tDMRG evolution, which ensures a well-controlled computational cost. The cost per time step scales as $O(\chi^3 d^3)$, where $d = 2S + 1$ is the local Hilbert space dimension. Although larger bond dimensions could improve accuracy, we verified in Appendix B that our chosen χ values yield converged results, balancing computational efficiency and spectral fidelity.

2. Real-time evolution using tDMRG

Following the computation of the ground state, the time evolution of the state produced by applying a local spin operator at the center of the chain was carried out using the tDMRG approach [28,29]. The evolution operator $U(t) = e^{-itH}$ was

approximated by decomposing it into Trotter gates [38–40]. For the spin-3/2 and spin-5/2 chains studied in this work, we consistently utilized Trotter gates with a time step of $0.05/J_1$, thus balancing computational efficiency and numerical accuracy. Throughout the evolution, the bond dimension of the resulting MPS was controlled by truncation, with the maximum allowed bond dimension being the same as that of the ground state.

The application of the local spin operator initially creates a local excitation in the center of the chain. In time, spin-spin correlations spread across the chain. To avoid boundary artifacts, we terminated the simulation once the correlations approached the chain edges. The maximum evolution time was chosen accordingly, with typical values around $t_f \approx 50/J_1$ to $20/J_1$ for spin-3/2 chains of length $N = 150$, and $t_f \approx 20/J_1$ to $12/J_1$ for spin-5/2 chains of length $N = 90$. The velocity of this correlation spread depends on the spin magnitude and is generally faster for higher spin values. As a result, in the spin-5/2 case, correlations reach the chain boundaries more quickly than in the spin-3/2 case.

B. Numerical computation and extraction of DSF

The DSF is obtained by means of a double Fourier transform of the calculated time-dependent spin-spin correlation functions. Due to simulations being performed for finite time intervals, numerical artifacts such as the "ringing" effects naturally occur in the Fourier transform. To mitigate these artifacts, the correlation functions were multiplied by a Gaussian filter $e^{-t^2/(2\sigma^2)}$ prior to performing the Fourier transform in time. We optimized the trade-off between energy resolution and numerical artifacts by choosing the Gaussian variance σ as $0.276t_f$.

The dynamical structure factor obtained from the t-DMRG method has the following Lehmann representation:

$$S^{zz}(k,\omega) = \frac{2\pi}{N}\sum_{\alpha} |\langle\psi_\alpha|S^z_{-k}|\psi_0\rangle|^2 \delta(\omega - \omega_\alpha(k)), \quad (2)$$

where $\omega_\alpha(k)$ represents excitation energies above the ground state. Since a local $S^\alpha_{r_i}$ operator can only connect states with total spin that differ by 1, and since the ground state lies in the total spin-singlet ($S_{\text{tot}} = 0$) sector, the operators S^z_{-k} connect it to triplet ($S_{\text{tot}} = 1$) excitations. Therefore, the lowest-energy peak in $S^{zz}(k,\omega)$ corresponds to the minimum energy in the $S_{\text{tot}} = 1$, $S^z_{\text{tot}} = 0$ sector.

The computational complexity grows substantially with increasing spin values due to larger local Hilbert spaces and increased entanglement entropy. Despite these challenges, our methodology remains robust, achieving convergence in the ground-state calculations and accurate real-time evolution for the spin-3/2 and spin-5/2 chains.

C. Ground-state *Ansatz*

For the spin-3/2 chain, our ground-state *Ansatz* for the partially dimerized phase in the valence bond picture is illustrated in Fig. 1(b). Each site is modeled as comprising three symmetrically coupled spin-1/2 particles. There exist two degenerate ground states, labeled GS1 and GS2. In GS1 (GS2), two singlet bonds form between neighboring sites on odd (even) bonds, and one singlet bond on even (odd) bonds.

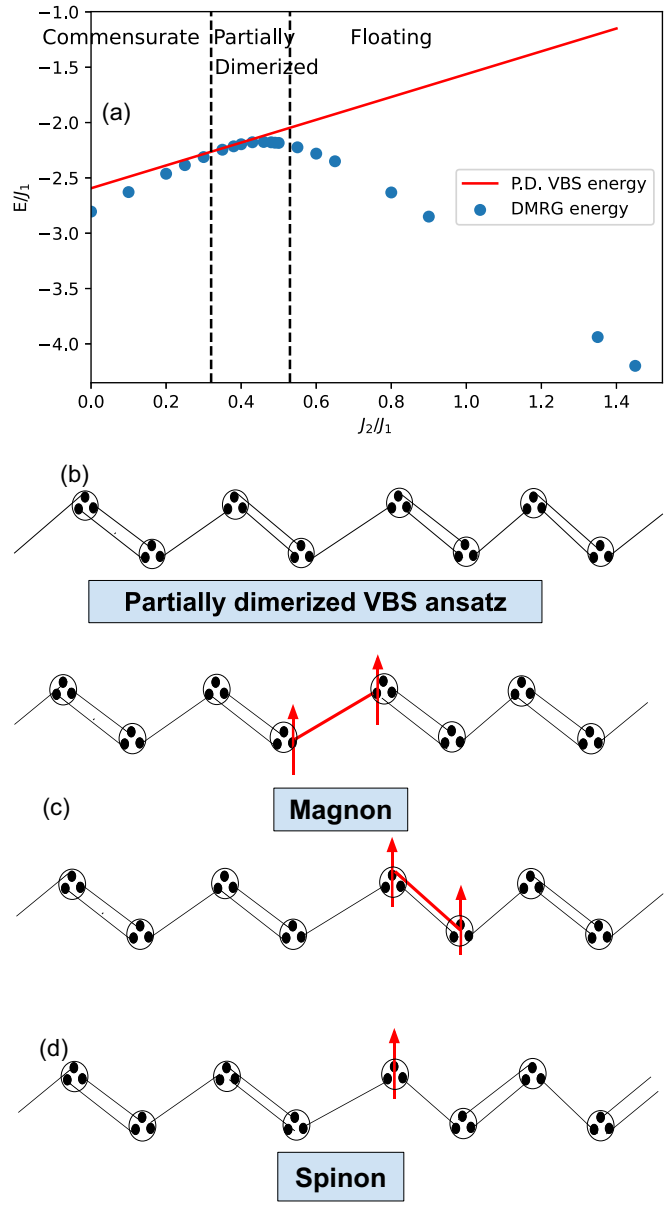

FIG. 1. (a) Comparison of partially dimerized VBS and DMRG ground-state energies (E/J_1), demonstrating the accuracy of the *Ansatz*. The dashed vertical lines indicate the approximate phase boundaries between the critical, partially dimerized, and floating phases. For spin-3/2, the values are adopted from Ref. [21]. (b) Illustration of the valence bond solid (VBS) *Ansatz* for the spin-3/2 J_1-J_2 Heisenberg chain, showing one of the two degenerate ground states. E denotes the ground-state energy. (c) Construction of magnon excitations by promoting singlet bonds into triplet states on different bonds. (d) Spinon excitation as a domain wall between the two VBS states, which are degenerate in the thermodynamic limit. Spinon excitations are always produced in pairs. Only one of the two excitations has been depicted. The second spinon, not shown, would appear as the other domain wall corresponding to an isolated spin further along the lower chain and is symmetrically equivalent to the first. Both spinons contribute additively to the total energy and momentum of the excitation.

Figure 1(a) validates this *Ansatz* by comparing the energy of the partially dimerized VBS state with the ground-state energy of the J_1-J_2 Heisenberg Hamiltonian obtained via DMRG simulations. The agreement between the two energies over the range $J_2/J_1 \in [0.3, 0.5]$ confirms the accuracy of the VBS *Ansatz* in describing the ground state in this regime.

A similar picture holds for the spin-5/2 case. The partially dimerized ground-state *Ansatz* now consists of alternating two and three singlet bonds on odd and even bonds, respectively, due to each site being composed of five symmetrically coupled spin-1/2 particles. The degenerate counterpart features two and three singlet bonds on even and odd bonds, respectively [see Fig. 2(b)].

Figure 2(a) confirms this *Ansatz* by comparing the variational energy with the DMRG ground-state results. The energies match closely in the vicinity of $J_2/J_1 \in [0.3, 0.4]$, again indicating the validity of the VBS construction in capturing the essential features of the partially dimerized phase in the spin-5/2 chain. Numerical studies in Ref. [22] indicate that a possible configuration like alternating one and four singlet bonds on even and odd bonds, respectively, is inconsistent with the local dimerization pattern observed in the true ground state of the spin-5/2 J_1-J_2 chain. This supports our chosen *Ansatz* as the physically relevant one, while ruling out competing dimerization patterns.

The energy difference between the VBS *Ansatz* and the DMRG ground state remains small in the commensurate, partially dimerized phase. However, as the system enters the floating phase, this discrepancy increases significantly. This can be understood by noting that our original VBS *Ansatz* is constructed with dimers on nearest-neighbor bonds. As J_2 becomes stronger, next-nearest-neighbor couplings become energetically favorable, and the true ground state develops longer-range singlet correlations. To explore this, we tested an alternative VBS *Ansatz* for the spin-3/2 chain, where dimers connect next-nearest-neighbor spins in an alternating pattern of one and two singlets per bond. This modified *Ansatz* yields lower energies in the floating phase and better agreement with DMRG results, supporting the idea that longer-range dimerization becomes more favorable in this regime (see Appendix C).

One can also observe that the VBS *Ansatz* performs better for the spin-3/2 chain than for the spin-5/2 case. This difference can be attributed to the fact that the parent Hamiltonian for the partially dimerized VBS state is structurally closer to the J_1-J_2 Heisenberg model in the spin-3/2 case. For higher-spin chains, the parent Hamiltonian of the dimerized state contains increasingly higher-order scalar products of neighboring spin operators, deviating further from the simple bilinear exchange form of the J_1-J_2 model. This trend is consistent with the known result that, for the spin-1/2 case, the Majumdar-Ghosh point lies exactly on the J_1-J_2 line, where the VBS state becomes an exact ground state. For a general construction of parent Hamiltonians for partially dimerized states with arbitrary half-integer spin, we refer the reader to Ref. [23].

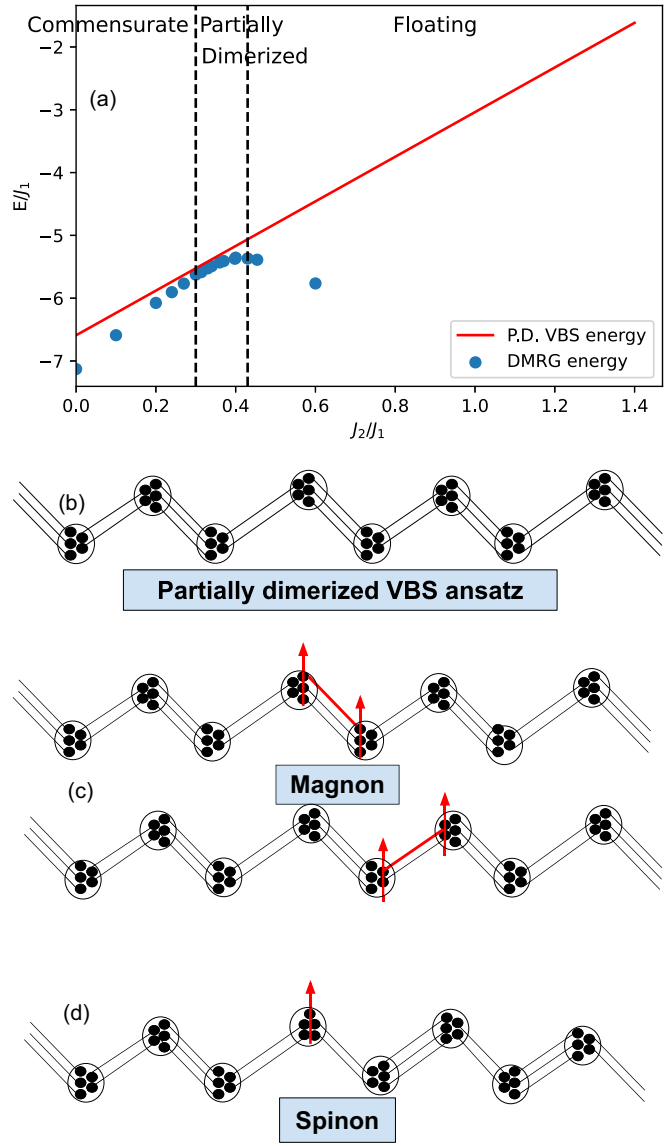

FIG. 2. Partially dimerized VBS *Ansatz* (b) and excitations for the spin-5/2 J_1-J_2 Heisenberg chain. Similar to Fig. 1, the VBS construction for magnon (c) and spinon (d) states is shown. The energy of the partially dimerized VBS state in panel (a) again matches closely with DMRG calculations in the partially dimerized phase, validating the *Ansatz* for higher-spin systems. The dashed vertical lines in panel (a) indicate the approximate phase boundaries between the critical, partially dimerized, and floating phases. Phase boundary values are taken from Ref. [22].

D. Excitations with SMA

Built on local variational excitations [41,42], the SMA is a valuable theoretical approach widely used to calculate the dispersion relations of local excitations in quantum many-body systems [30,31,41]. Originally developed in the context of quantum fluids, the SMA was later successfully extended to quantum spin chains, most notably to describe magnon dispersion in VBS states such as the Affleck-Kennedy-Lieb-Tasaki (AKLT) model [32,33]. Given that the DMRG provides highly accurate ground states expressed naturally in MPS

form, the SMA framework can be seamlessly generalized to MPS ground states to systematically compute the magnon and spinon dispersion relations.

For a local excitation with momentum k in a chain of length N, the SMA state is defined as

$$|k\rangle = \frac{1}{\sqrt{N}} \sum_{j=1}^{N} e^{ikr_j}\, \Omega_j |\psi_0\rangle, \tag{3}$$

where the operator Ω_j creates a local perturbation (such as a bond flip from a singlet to a triplet) at bond (or site) j on the ground state $|\psi_0\rangle$. The dispersion relation for this excitation, $\omega(k)$, is obtained straightforwardly from

$$\omega(k) = \frac{\langle k|\, H\, |k\rangle}{\langle k|k\rangle} - E_0, \tag{4}$$

where E_0 is the energy of the ground state. Upon expanding the exponentials in Eq. (4) in terms of trigonometric functions, one obtains

$$\omega(k) = \frac{a_0 + \sum_{n=1}^{N/2} a_n \cos(nk)}{1 + \sum_{n=1}^{N/2} b_n \cos(nk)} - E_0, \tag{5}$$

where a_n and b_n are parameters determined by matrix elements involving the Hamiltonian and overlaps between the states with the quasiparticle localized at different positions.

For the spin-3/2 and spin-5/2 J_1-J_2 Heisenberg chains considered in this study, we employ SMA to systematically analyze two primary classes of excitations relevant to the interpretation of the DSF spectra.

(1) *Magnon excitations.* In the partially dimerized phase, the ground state can be effectively represented as a VBS state consisting of one or two singlet bonds arranged periodically for the spin-3/2 chain, and two or three singlet bonds for the spin-5/2 chain. A local triplon excitation corresponds to promoting one of these singlet bonds to a triplet, as illustrated schematically in Fig. 1(c) for spin-3/2 and in Fig. 2(c) for spin-5/2. When such an excitation propagates coherently with a well-defined momentum k, it gives rise to a magnon mode [33]. We construct explicit magnon states by introducing such local bond-flips into the partially dimerized VBS state. The resulting dispersion relations, computed via SMA, allow direct comparisons with numerically calculated DSF spectra, enabling the identification of distinct magnon features.

(2) *Spinon (domain-wall) excitations.* Another fundamental class of excitations arises from domain walls separating two degenerate partially dimerized states, which are related by a one-site translation, as illustrated in Fig. 1(d) for spin-3/2 and in Fig. 2(d) for spin-5/2. Unlike magnons, these domain-wall excitations carry fractionalized spin quantum numbers (half integers) and are therefore classified as spinons [6]. Generating spinon states directly in an MPS framework involves nonlocal transformations, making analytical expressions difficult. Nevertheless, the SMA allows for the numerical construction and systematic study of spinon dispersions by carefully preparing VBS states featuring domain walls. It is crucial to recognize that because of the dimerized nature of the state, spinons hop over every other lattice site; thus, care must be taken to properly account for this periodicity when performing the Fourier transform to momentum space. The analysis of spinon dispersions provides important insights into fractionalization phenomena near quantum phase transitions, which is particularly relevant for frustrated spin chains.

Employing the SMA to examine these two excitation types has allowed us to develop comprehensive interpretations of DSF features, deepening our understanding of the interplay between magnons and spinons in spin-3/2 and spin-5/2 Heisenberg chains.

Since the spinons are always produced in pairs and are free to move in the chain, there is a continuum in the spectral function. The continuum is characterized by the combined contributions of each spinon, and their total momentum and energy are given by

$$K = (k_1 + k_2) \mod 2\pi, \quad E_K = E_{k_1} + E_{k_2},$$

where k_1 and k_2 are the wave vectors of the individual spinons, and E_{k_1} and E_{k_2} are their respective energies.

In constructing the VBS *Ansatz* for the excited states analyzed here, we adopted a matrix product state (MPS) based approach, as described in detail in Ref. [19].

III. RESULTS

A. DSF of the spin-3/2 J_1-J_2 chains

In this section, we report on the DSF of spin-3/2 J_1-J_2 chains using extensive numerical simulations via tDMRG. The DSFs for various values of the next-nearest-neighbor coupling J_2 are presented in Figs. 3(a)–3(f) , providing a broad perspective on the evolution of the spectral functions across different phases.

At low values of J_2, specifically at $J_2 = 0.2J_1$, the spin-3/2 chain resides within a critical phase (C) characterized by gapless spin excitations. The DSF clearly exhibits a continuum with spectral boundaries consistent with the well-known de Cloiseaux-Pearson dispersion form [43], indicative of spinon-like fractional excitations. This continuum is typical for critical quantum spin chains and aligns with theoretical expectations of the spectra in a quantum critical phase.

Upon increasing J_2, the model transitions into a partially dimerized VBS phase, exhibiting a spectral gap. Within this phase, as J_2 further increases ($J_2 = 0.35J_1$ to $0.5J_1$), the DSF evolves into a richer structure with distinct features emerging at higher energies. Notably, within this intermediate-parameter regime, the spin-spin correlation function becomes incommensurate, clearly reflected in the DSF as the low-energy excitation boundary develops two minima at incommensurate momenta.

At still larger J_2 values (e.g., $J_2 = 0.65J_1$), the spin-3/2 system exits the dimerized phase and reenters another critical phase (floating phase), as evidenced by the return of a gapless spectrum reminiscent of the initial critical region. The DSF spectrum at this higher J_2 value looks like the superposition of two de Cloiseaux-Pearson continua [43] touching zero energy at incommensurate wave vectors. This is in line with the expectation that, for $J_1 = 0$, the DSF will be the superposition of two spin-3/2 DSFs with a double unit cell, hence with a minimum at $\pi/2$.

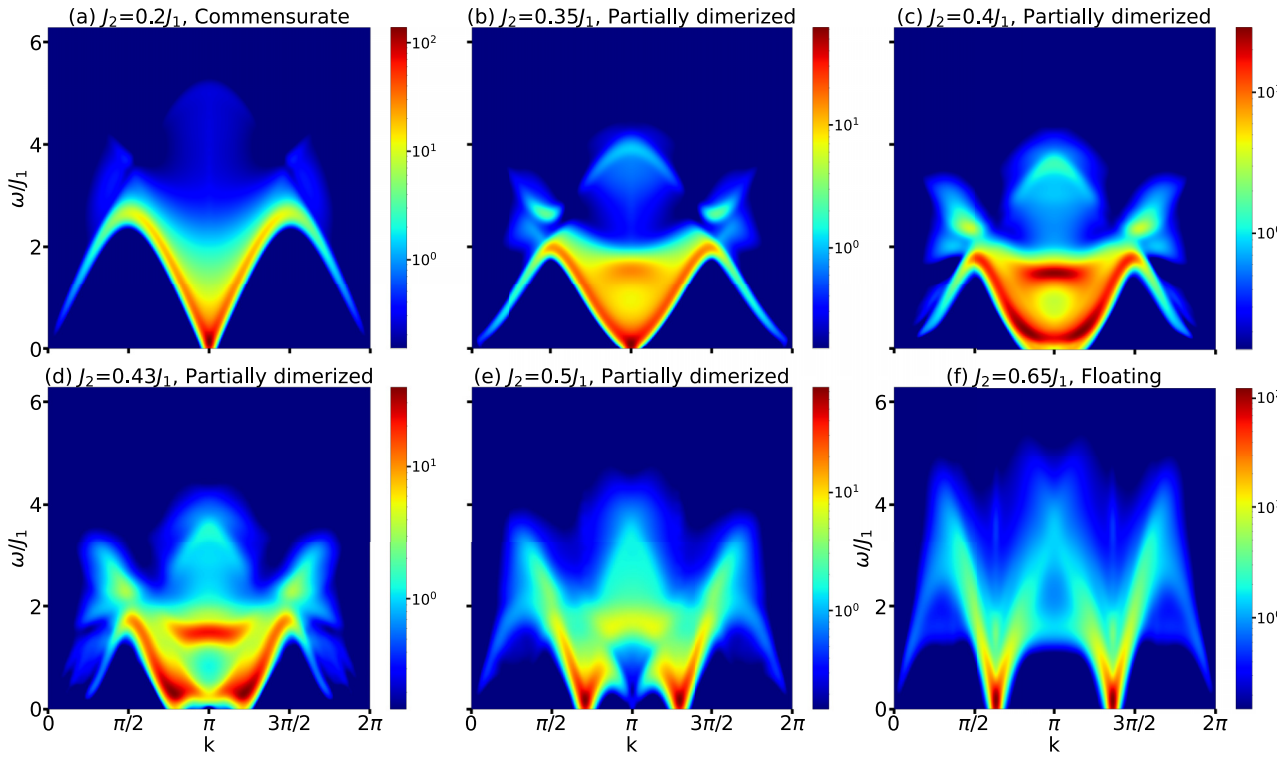

FIG. 3. Dynamical structure factor $S^{zz}(k, \omega)$ of the spin-3/2 J_1-J_2 chain at increasing values of J_2. As J_2 increases, the system transitions from (a) a gapless critical phase into (b)–(e) a gapped partially dimerized phase, and (f) reenters into a critical incommensurate phase. The emergence of incommensurate correlations is signaled by the splitting of low-energy spectral features.

B. SMA analysis of spin-3/2 J_1-J_2 chains

To provide deeper insights into the spectral features observed in the DSFs of the spin-3/2 J_1-J_2 chain models, we conducted a comprehensive analysis using the SMA. Specifically, we focused on understanding the spectral contributions from spinon and magnon excitations within the partially dimerized phase.

We first examined the spinon excitations associated with domain walls separating two degenerate partially dimerized states, which differ by a translation of one lattice site. Using the SMA, we calculated the spinon dispersion and subsequently obtained the two-spinon continuum. In Fig. 4(a), we compare the computed two-spinon continuum (shaded green region, right panel) to the corresponding DSF data (left panel). Remarkably, the spinon continuum qualitatively reproduces key features of the DSF spectra across a range of parameters, strongly suggesting that fractional spinon excitations play a dominant role in determining the spectral characteristics of the J_1-J_2 spin 3/2.

In parallel, we performed SMA calculations for magnon excitations on the partially dimerized ground state by explicitly breaking a singlet bond and converting it into a triplet bond, thus forming a local quasiparticle excitation. The resulting magnon dispersions (white solid curves) are also plotted on top of the DSF data in Fig. 4(a). We observe that the magnon dispersion curves pass through several regions of high spectral intensity in the DSFs, indicating that magnon-like excitations are indeed present. However, given their embedding within the extensive spinon continuum, these magnons likely appear as resonant modes rather than stable, isolated quasiparticles, suggesting complex magnon-spinon interactions.

To further elucidate the behavior of spinon excitations, we present separately the calculated spinon dispersions in Fig. 4(b). A notable feature of these dispersions is the progressive splitting of the dispersion minima as the system enters the incommensurate regime, clearly signaling the onset of incommensurate correlations. Additionally, the spinon gap initially increases, reaches a maximum, and subsequently decreases with increasing J_2, providing direct evidence of nontrivial spectral behavior near quantum phase transitions between the commensurate critical and incommensurate floating phase.

To gain a deeper theoretical understanding of the incommensurate features observed in the spinon dispersion, we reinterpret the SMA-derived dispersion in terms of an effective tight-binding model. In the SMA framework, the excitation energy is computed using Eq. (5). One can define $\mathcal{O}_{ij} = \langle\Omega_j|\Omega_i\rangle$ as the overlap matrix, with $|\Omega_j\rangle$ denoting a state with local spinon excitation at the site j. Since these states are not orthogonal, the resulting subspace is nontrivial and must be handled carefully.

We now reinterpret the dispersion calculation as a variational problem within the subspace spanned by the nonorthogonal basis $\{|\Omega_i\rangle\}$. The effective Hamiltonian $\tilde{H}$, acting within this subspace, is defined as

$$[\tilde{\mathcal{H}}]_{ij} = \sum_k [\mathcal{O}^{-1}]_{ik} \langle\Omega_k|\mathcal{H}|\Omega_j\rangle. \tag{6}$$

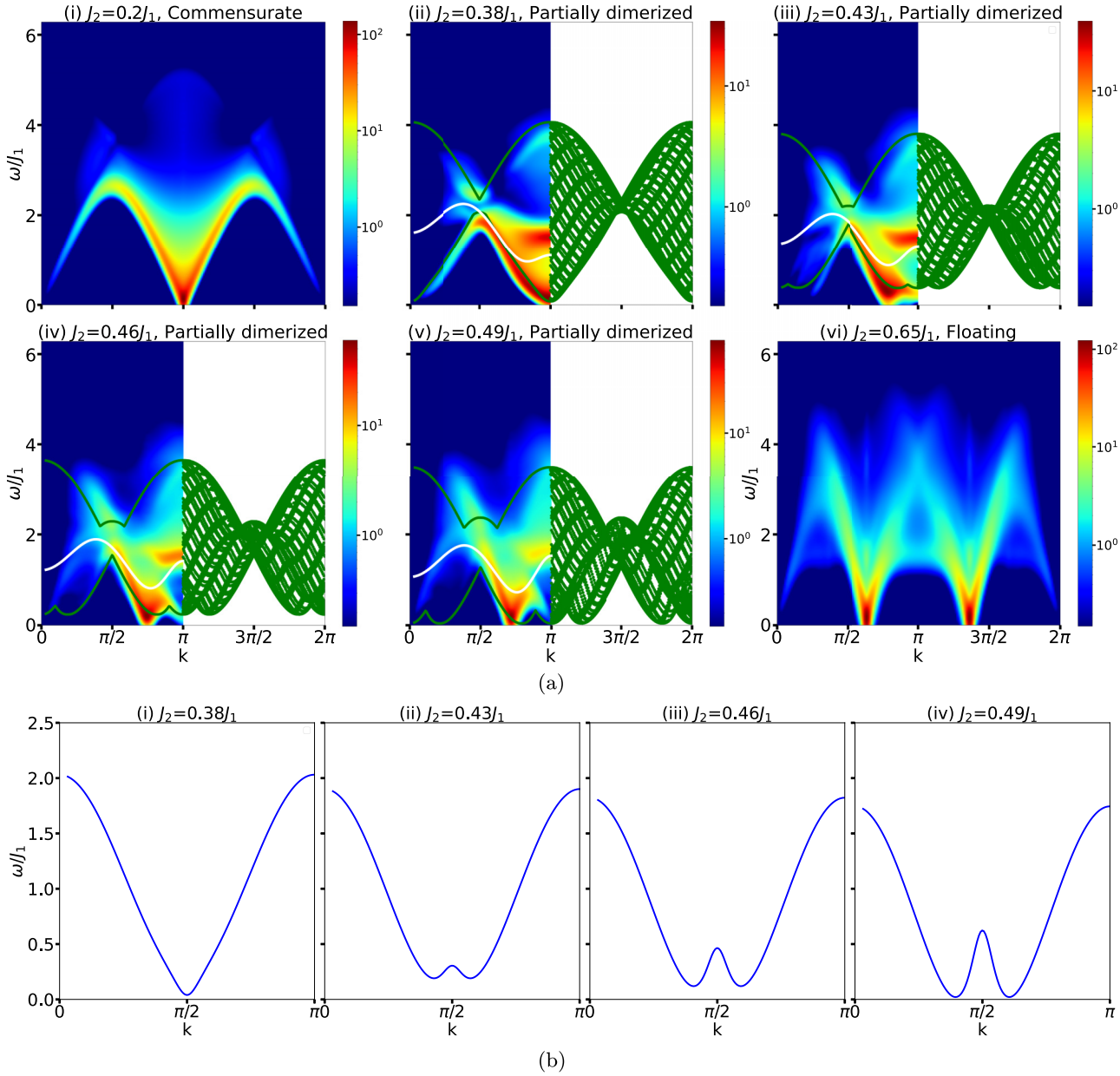

FIG. 4. (a) Dynamical structure factors for spin-3/2 chains compared with two-spinon continua (green shaded regions) calculated from the spinon dispersion of the domain-wall excitation between two degenerate partially dimerized states. The green boundaries superimposed on the DSFs trace the edges of the continuum. The magnon dispersion (white solid curves), obtained via SMA on the partially dimerized state, is also shown. The SMA magnon dispersions pass through high spectral-intensity regions that are likely to be resonant magnons within the spinon continuum. (b) Corresponding spinon dispersions highlighting the splitting of dispersion minima as a clear sign of the onset of incommensurability, with the spinon gap showing nonmonotonic behavior as J_2 is varied.

The generalized eigenvalue problem,

$$\sum_j \tilde{H}_{ij}\psi_j = \omega \sum_j \mathcal{O}_{ij}\psi_j, \tag{7}$$

yields the spinon dispersion through the spectrum of $\tilde{H}$. By performing a basis transformation using the inverse of the overlap matrix, $\mathcal{O}^{-1}$, this is equivalent to diagonalizing the projected Hamiltonian PHP, where P projects onto the variational subspace.

In this representation, the energy dispersion can be written as

$$\omega(k) = \gamma_0 + \sum_{n=1}^{N/2-1} 2\gamma_n \cos(kn), \tag{8}$$

where the coefficients $\gamma_n = \langle \Omega_{N/2} | \tilde{H} | \Omega_{N/2+n} \rangle$ can be interpreted as effective hopping amplitudes in a tight-binding model. Here, n denotes the distance between spinon positions. A more detailed exposition of this construction can be found

TABLE I. Effective tight-binding hopping amplitudes γ_n (in units of 10^{-2}) extracted from the SMA spinon dispersions for various values of J_2/J_1.

J_2/J_1	γ_0	γ_2	γ_4	γ_6	γ_8	γ_{10}	γ_{12}	γ_{14}	γ_{16}
0.38	112	47.0	−2.31	1.54	−1.03	0.686	−0.457	0.305	−0.203
0.43	97.8	44.1	3.47	−2.31	1.54	−1.03	0.686	−0.457	0.305
0.49	80.9	40.5	10.4	−6.94	4.63	−3.09	2.06	−1.37	0.914

in Refs. [6,19], where it was successfully applied to domain-wall excitations in spin-1/2 and spin-1 Heisenberg chains.

As noted previously in Sec. II D, spinon propagation occurs on every other site due to the underlying dimerized structure of the ground state. As a consequence, the effective hopping amplitudes γ_n vanish for all odd n, and only even-n contributions survive in Eq. (8).

We have computed γ_n values numerically for several ratios J_2/J_1, with the leading nonzero values shown in Table I. At $J_2/J_1 = 0.38$, the spinon dispersion exhibits a single minimum at $k = \pi/2$, indicating commensurate behavior. In this case, the second and fourth neighbor hoppings (γ_2, γ_4) exhibit alternating signs, with γ_4 being small and negative. This sign alternation ensures that the different cosine terms in Eq. (8) reinforce the same momentum minimum, stabilizing the commensurate dispersion. This pattern of alternating signs persists for all further-neighbor hoppings, with a diminishing amplitude, as illustrated in Fig. 5.

However, as J_2/J_1 increases, γ_4 becomes positive while γ_2 remains positive, leading to constructive interference of multiple cosine terms in Eq. (8). This competition between hopping amplitudes introduces a double-minimum structure in the spinon dispersion, manifesting as incommensurate modes. At $J_2/J_1 = 0.43$, a weak splitting appears, with γ_4 approximately one-tenth of γ_2. This splitting becomes more pronounced at $J_2/J_1 = 0.49$, where γ_4 grows to roughly one-fourth of γ_2, enhancing the competition and pushing the minima further away from $k = \pi/2$.

This tight-binding reinterpretation of the SMA dispersion makes the mechanism behind the incommensurability explicit: the interplay between second- and higher-neighbor hopping amplitudes destabilizes the commensurate minimum and leads to the emergence of incommensurate excitations.

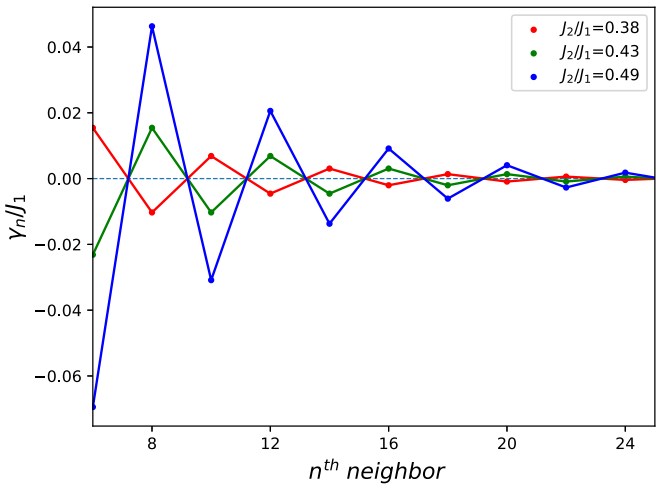

FIG. 5. Effective tight-binding hopping amplitudes γ_n (in units of J_1) extracted from the SMA spinon dispersions for several ratios J_2/J_1. Only even-n terms appear because the spinon domain wall can propagate only between alternating sites of the underlying VBS state.

C. DSF and SMA analysis of the spin-5/2 J_1-J_2 models

We now extend our study of the DSF to the spin-5/2 J_1-J_2 Heisenberg chain, using tDMRG simulations and SMA analysis. Figure 6 presents the DSFs for increasing values of J_2. It captures the evolution of the spectral response as the system transitions through distinct quantum phases.

At small J_2, the system exhibits a gapless commensurate critical phase and, as for spin-3/2, the spectral functions are reminiscent of the de Cloiseaux-Pearson continuum [43], a characteristic of fractional spinon excitations. Upon increasing J_2, the system enters a partially dimerized regime, where a spin gap opens and the DSF develops more structured intensity distributions. As J_2 increases further, incommensurate features emerge, visible through the splitting of low-energy spectral peaks. Eventually, at large J_2, the system enters a floating incommensurate phase, characterized by gapless excitations with incommensurate momenta, manifesting as a broad continuum in the DSF similar to the spin-3/2 chain.

To understand the nature of low-energy excitations in the partially dimerized phase, we carry out an SMA analysis on VBS states for both spinon and magnon modes, following the procedure established for the spin-3/2 chain. As in that case, spinon excitations correspond to domain walls between two degenerate partially dimerized VBS states. We construct spinon dispersions and compare in Fig. 7(a) the two-spinon continuum (green shaded region, right panel) with the DSF data (left panel). The close match between the continuum and regions of significant spectral intensity strongly suggests that fractionalized spinon excitations dominate low-energy dynamics.

Magnon excitations, constructed by locally promoting a singlet bond into a triplet, are also analyzed within the SMA framework. The resulting magnon dispersion relations are shown as white lines in Fig. 7(a). These modes traverse regions of high spectral weight, indicating their relevance as coherent, resonant excitations, even if embedded within a broader spinon continuum. As in the spin-3/2 case, this coexistence underscores the complex interplay between fractional and collective excitations in higher-spin chains.

Figure 7(b) displays the calculated spinon dispersions, which exhibit clear incommensurate minima and nonmonotonic gap evolution with increasing J_2. These features confirm the onset of incommensurate correlations within the partially dimerized phase and highlight the proximity to floating phase physics.

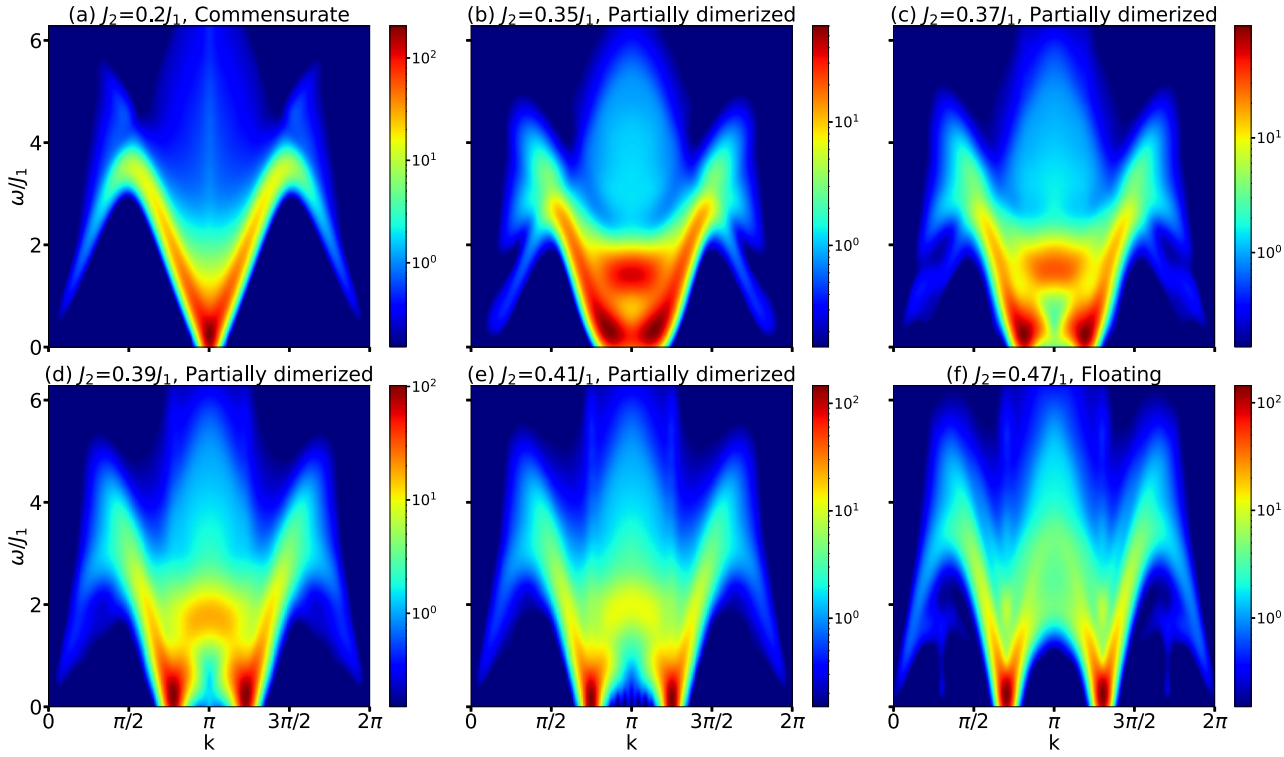

FIG. 6. Dynamical structure factor $S^{zz}(k, \omega)$ of the spin-5/2 J_1-J_2 Heisenberg chain at increasing values of J_2. As J_2 increases, the system transitions from (a) a gapless commensurate phase into (b)–(e) a gapped partially dimerized regime, and then into (f) a gapless incommensurate (floating) phase. The onset of incommensurate correlations is visible in the splitting and broadening of low-energy spectral features.

Together, the tDMRG and SMA results reveal a consistent picture: the spin-5/2 J_1-J_2 chain supports a partially dimerized intermediate phase, and its low-energy excitations are mainly fractionalized spinons.

IV. INTERPRETATION OF THE RESULTS

In this section, we summarize and interpret the key phenomenological trends observed in our numerical simulations and analytical calculations, with a particular focus on the evolution of spectral features across different coupling regimes in both spin-3/2 and spin-5/2 chains.

The transition into incommensurate correlations is captured through the wave vector evolution of both spinon and magnon dispersions. The quantity q plotted in Fig. 8 represents the wave vector at which the lowest-energy excitation occurs in the SMA dispersion for magnons or the two-spinon continua. At small values of J_2/J_1, the dispersion minimum is located at $k = \pi$, consistent with commensurate correlations. As J_2 increases, this minimum splits into two symmetric incommensurate minima that gradually separate from $k = \pi$, signaling the onset and evolution of incommensurate correlations. The plotted q values correspond to the positions of these incommensurate minima and are numerically extracted from the SMA dispersion. The estimates shown in Fig. 8 (e.g., the onset of incommensurability at $J_2/J_1 \approx 0.32$ and 0.4) are based on single-mode approximation (SMA) dispersions derived from variational valence bond solid (VBS) *Ansätze*. Since these *Ansätze* are constructed in the thermodynamic limit and the SMA formulation is analytical, the resulting dispersion minima are expected to be insensitive to system size if the lattice size is large enough. In our calculations, we used a chain length of $L = 200$ sites for both spinon and magnon dispersions in the spin-3/2 case, $L = 200$ for spinon dispersions in the spin-5/2 case, and $L = 300$ for magnons in the spin-5/2 chain. We verified the stability of these estimates by repeating the SMA dispersion calculations at multiple system sizes exceeding these values. At representative values of J_2/J_1, we found that the momentum q at which the lowest excitation occurs does not shift with increasing system size, confirming that our incommensurability estimates are intrinsic and converged. Figure 8(a) presents a comparison of wave vectors as functions of J_2 for the magnon, and spinon continua, for spin-3/2 chains. The magnon dispersion becomes incommensurate at $J_2 \approx 0.32J_1$. In contrast, the spinon dispersion becomes incommensurate at a later value, approximately $J_2 \approx 0.4J_1$. According to Ref. [24], the Lifshitz point occurs at $J_2 \approx 0.388J_1$, where the static structure factor develops two distinct peaks. This intermediate window, in which the spinon dispersion becomes incommensurate while the magnon dispersion remains commensurate, spans the region around the Lifshitz point at $J_2 \approx 0.388J_1$ and highlights a subtle competition between two mechanisms of incommensuration: one driven by magnon propagation and the other by the underlying spinon domain-wall excitations. Although magnons appear as well-defined modes in the SMA calculations, their signatures in the DSF suggest that they are not isolated quasiparticles. Rather, their dispersions traverse regions of high spectral weight within the broader spinon continuum, indicating that these magnons may be viewed as resonances–collective modes dressed by the surrounding

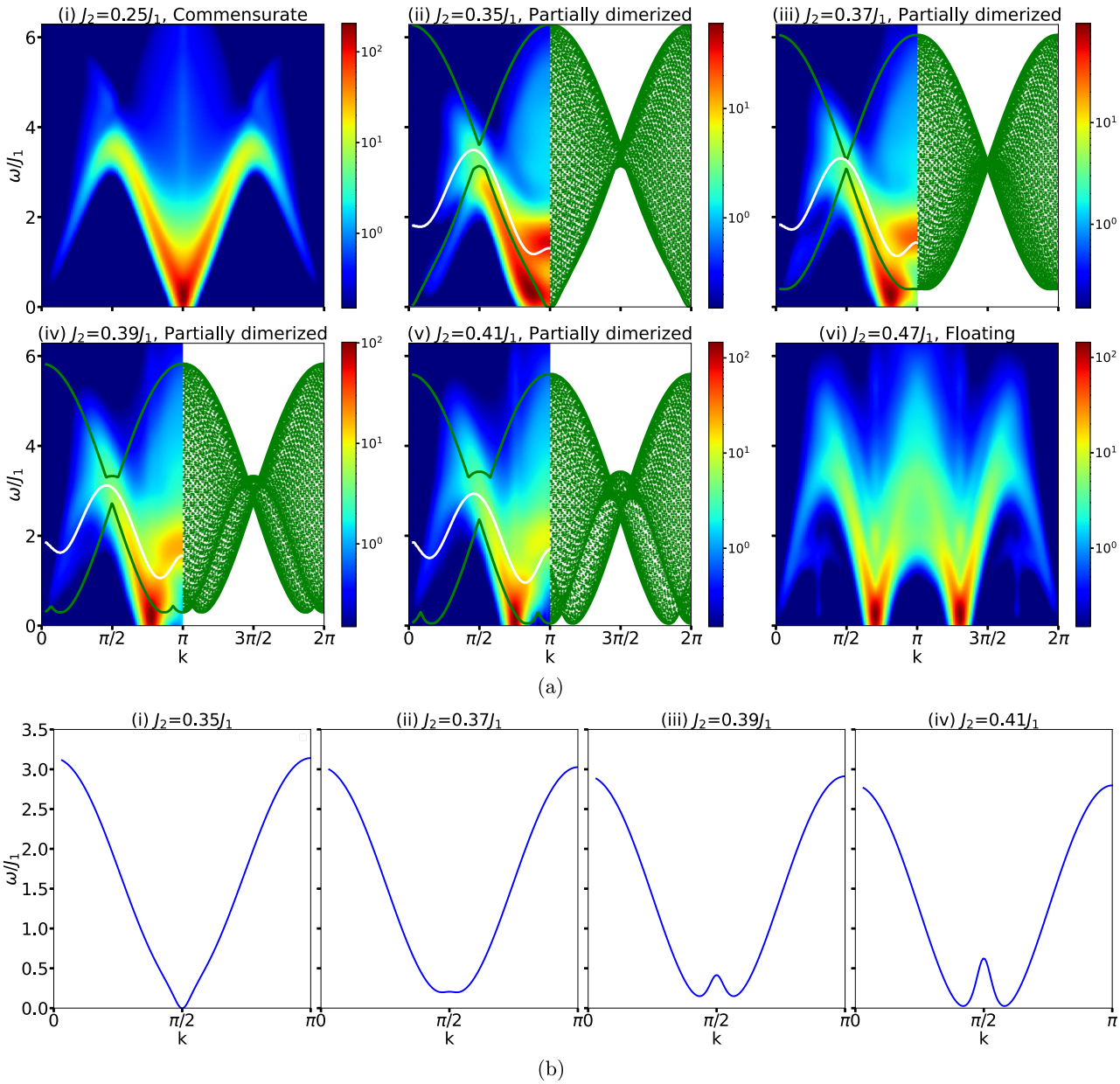

FIG. 7. (a) Dynamical structure factors of the spin-5/2 J_1-J_2 chain compared with two-spinon continua (green) and SMA-derived magnon dispersions (solid lines). The green boundaries superimposed on the DSFs trace the edges of the continuum. Magnons follow regions of high spectral weight. (b) Spinon dispersions exhibit incommensurate minima and nonmonotonic gap variation with J_2.

fractional excitations. Indeed, the minimum of the magnon dispersion at an incommensurate value of the wave vector is reflected in the dispersion of a broad resonance, as can be seen in Fig. 4(a)(iv). This interpretation underscores the hybrid nature of excitations in frustrated systems, where the distinction between quasiparticles and continua becomes blurred by strong correlations.

A similar scenario emerges for the spin-5/2 chain, as illustrated in Fig. 8(b). Here, the magnon dispersion becomes incommensurate at $J_2 \approx 0.32J_1$, closely followed by numerical incommensuration at $J_2 \approx 0.33J_1$ [22], and the spinon dispersion becomes incommensurate at a slightly higher coupling of $J_2 \approx 0.36J_1$. This indicates a universal pattern in higher-spin frustrated quantum chains, with quantitative differences emerging due to the reduced quantum fluctuations and altered interplay of spin excitations at higher spin magnitudes.

In both the spin-3/2 and spin-5/2 cases, when increasing J_2/J_1 the spinon dispersion reaches zero with splitting, as illustrated in Figs. 4(b) and 7(b). This behavior is indicative of a condensation of incommensurate spinons, heralding the emergence of the floating phase.

Overall, the SMA framework, supported by high-precision tDMRG data, successfully disentangles the spectral landscape of the DSF into its elementary constituents, spinons, and magnons, thereby providing a detailed microscopic understanding of the rich dynamical behavior of the frustrated spin chains.

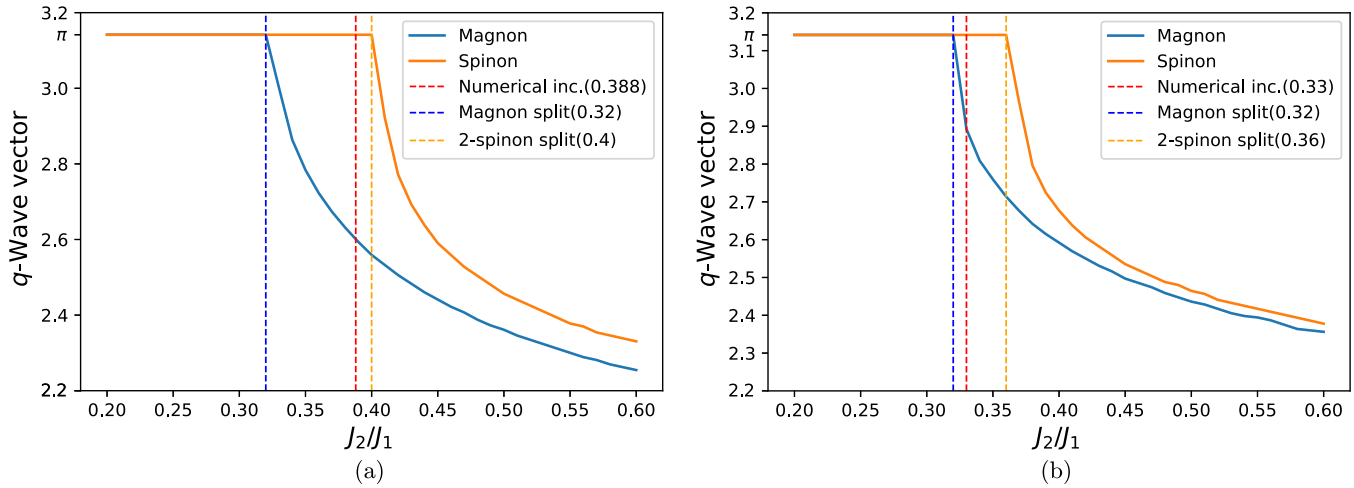

FIG. 8. (a), (b) Comparison of wave vectors as functions of J_2 for magnon and spinon continua in spin-3/2 and spin-5/2 chains, respectively. The plot highlights the transitions into incommensurate behavior for both spin chains.

V. CONCLUSION AND DISCUSSION

In this work, we have performed a comprehensive study of the DSF of the frustrated spin-3/2 and spin-5/2 Heisenberg chains governed by the J_1-J_2 model. Focusing on the partially dimerized phase and its adjacent transitions, we investigated the nature of low-lying excitations and their contributions to the DSF using a combination of numerical and analytical techniques. Leveraging the high accuracy of the DMRG and tDMRG methods, alongside analytical insight from the SMA, we identified the distinct roles of magnon and spinon excitations in shaping the observed spectral features.

Our results provide a deeper understanding of frustrated quantum magnetism, shedding light on the emergence of incommensurability in the DSF and its implications for experimental observations. Across both spin-3/2 and spin-5/2 cases, the spectral function is dominated by spinon continua, similar to the spin-1/2 case, and the magnon mode remains within the two-spinon continuum throughout the Brillouin zone, as visible in our DSF data in Figs. 3 and 6.[1] This contrasts with the spin-1/2 Majumdar-Ghosh point [4] at $J_2/J_1 = 0.5$, where the magnon briefly detaches near $k = \pi/2$. Furthermore, the SMA-derived spinon dispersion undergoes a transition to incommensurability as J_2 increases. The gap of the spinon modes closes on both sides of the partially dimerized phase. At the lower boundary, the spinon mode condenses at the commensurate wave vector $k = \pi/2$, leading to a standard Luttinger liquid phase with central charge $c = 1$. In contrast, at the upper boundary, the condensation takes place simultaneously at two incommensurate wave vectors, leading to a DSF with two gapless continuous modes. This suggests that the central charge $c = 2$, as in the limit of decoupled chains ($J_1 = 0$). Further numerical verification of this prediction, however, is extremely challenging due to incommensurate Friedel oscillations affecting the finite-size entanglement entropy profile [44,45]. We emphasize that our SMA calculations are intended solely to provide a qualitative explanation of the features observed in our DSF results. The SMA construction is based on a variational *Ansatz* and cannot be used to definitively establish the existence or nature of these critical phases. In particular, similar features may appear in simpler systems (e.g., the spin-1/2 chain) where no floating phase is known to exist. The presence and characterization of the floating phase are more reliably supported by independent DMRG analyses (see, e.g., Refs. [21,22]), which are beyond the resolution of the present SMA-based approach.

Furthermore, our predictions for the DSF can be considered as predictions for the inelastic neutron-scattering spectrum of frustrated spin chains. For instance, Bi_3 $FeMo_2$ O_{12} is believed to be well described by the spin-5/2 J_1-J_2 model with $J_2/J_1 \simeq 1$ [46]. Our approach predicts that the spectrum should consist of a double Des Cloizeaux-Pearson continuum that touches zero energy at a slightly incommensurate wave vector [22]. It would be interesting to check if other systems could be found that lie in the intermediate gapped region for which the DSF exhibits a richer structure.

On the methodological side, our use of the SMA on both magnons and spinons has proven to be an effective tool in disentangling contributions to the DSF. While the magnons do not fully explain the DSF on their own, their dispersion curves coincide with regions of high spectral weight, suggesting that they may manifest themselves as resonances within the broader spinon continuum. This subtlety adds depth to the understanding of spectral mixing in frustrated spin systems, particularly in regimes with strong quantum fluctuations. We emphasize that the SMA-based construction provides a qualitative and variational interpretation of the excitations, particularly in the partially dimerized phase.

Unlike the $S = 1/2$ Majumdar-Ghosh point, there is no value of J_2 where our VBS *Ansatz* becomes exact for higher spin. Thus, our conclusions regarding magnon and spinon mode spectral features are approximate and should be interpreted with this limitation in mind.

[1] However, we cannot entirely rule out the presence of a two-spinon bound state in the triplet sector based on the present DSF data shown in Figs. 3 and 6, as the resolution is limited by finite chain sizes and the finite time of the real-time evolution. A more precise identification of such a bound state would require a dedicated analysis beyond the SMA, analogous to approaches used in the spin-1/2 case [6].

The framework we developed, combining VBS intuition with SMA and tDMRG, can be readily extended to other frustrated or topologically nontrivial spin systems. Future directions include the extension of this approach to the spin chains with three-site interactions, or two-dimensional analogs such as frustrated ladders and square lattices.

ACKNOWLEDGMENTS

We thank Henrik M. Rønnow for insightful discussions. A.S. acknowledges support from the Swiss Government Excellence Scholarship (FCS Grant No. 2021.0414). This work was supported by the Swiss National Science Foundation under Grants No. 212082 and No. 188648. The calculations have been performed using the facilities of the Scientific IT and Application Support Center of EPFL.

DATA AVAILABILITY

The data that support the findings of this article are not publicly available upon publication because it is not technically feasible and/or the cost of preparing, depositing, and hosting the data would be prohibitive within the terms of this research project. The data are available from the authors upon reasonable request.

APPENDIX A: ESTIMATION OF CORRELATION LENGTHS

To ensure that the chosen system sizes for the calculation of the dynamical structure factor are sufficiently large, we estimated the spin–spin correlation lengths for a few parameters under investigation. The correlation lengths were extracted by fitting the equal-time spin–spin correlation function envelope to the Ornstein-Zernike form [47,48]

$$C^{\mathrm{OZ}}_{i,j} \propto \frac{e^{-|i-j|/\xi}}{\sqrt{|i-j|}}, \tag{A1}$$

where ξ denotes the correlation length.

The numerical correlation data were fitted to this expression in logarithmic form, which linearizes the exponential decay and provides a more stable estimate for ξ. Only the envelope was considered in the fit, which effectively neglects the oscillatory contributions and isolates the exponential decay behavior.

For the spin-3/2 Heisenberg chain at $J_2 = 0.38$ and $J_2 = 0.43$, the extracted correlation lengths are $\xi \approx 4.38$ and $\xi \approx 5.15$, respectively [Figs. 9(a) and 9(b)], calculated on a chain of 150 sites. Similarly, for the spin-5/2 Heisenberg chain at $J_2 = 0.36$, we find a correlation length of $\xi \approx 7.51$ [Fig. 9(c)], calculated on a chain of 90 sites. All these systems are located in gapped phases, and the finite values of ξ confirm the presence of an excitation gap and short-range spin correlations. To estimate fitting uncertainties and validate the robustness of our procedure, we repeated the fits using only the local maxima (peaks) of the correlation function. When the number of oscillation periods is large because it is in our system of $L = 150$ sites, both fitting procedures should converge to the same value. We indeed find close agreement: the peak-based fit yields $\xi \approx 4.38$ and $\xi \approx 5.11$ for spin-3/2 at $J_2 = 0.38$ and $J_2 = 0.43$, respectively, and $\xi \approx 7.22$ for spin-5/2 at $J_2 = 0.36$. The difference between these two estimates can be interpreted as a rough estimate of the fitting uncertainty for a given system size.

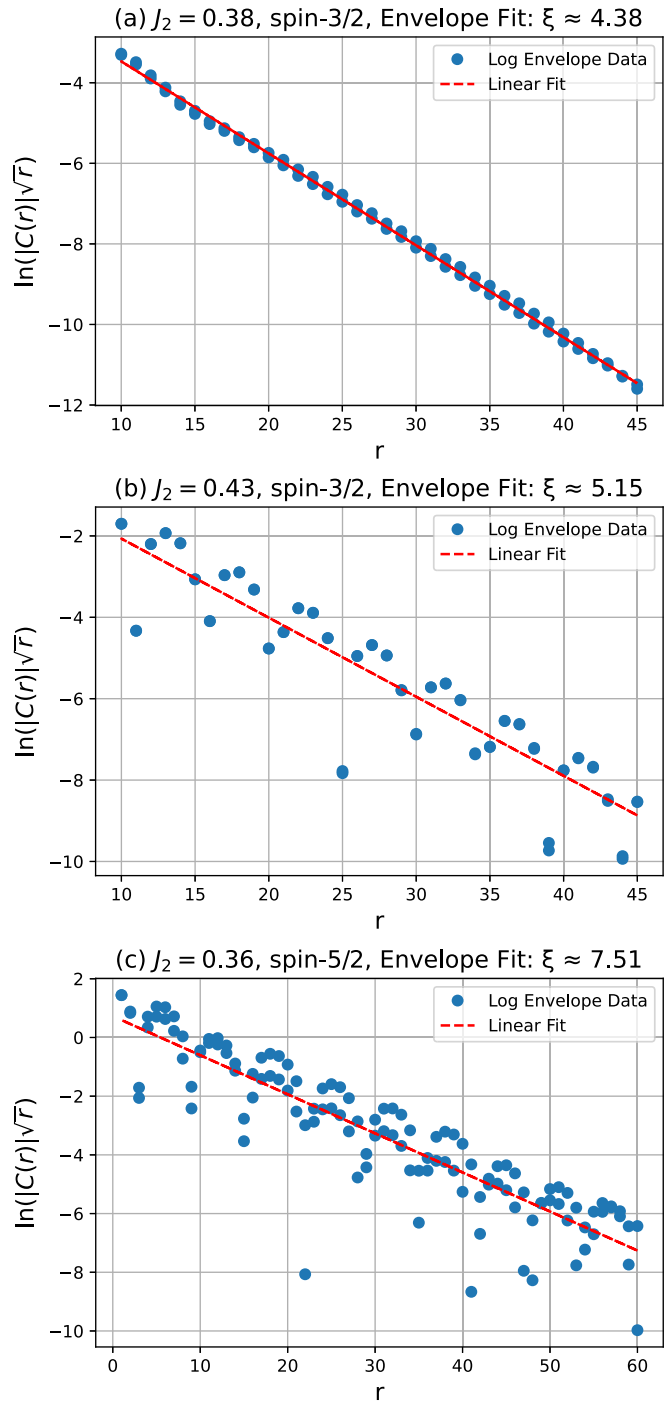

FIG. 9. Correlation envelope fits for different values of J_2 and spin magnitude. (a) $J_2 = 0.38$, spin 3/2; (b) $J_2 = 0.43$, spin 3/2; (c) $J_2 = 0.36$, spin 5/2.

The system sizes employed for the dynamical structure factor calculations were chosen to be significantly larger than these correlation lengths, ensuring that finite-size effects are well controlled and the extracted spectra are physically meaningful.

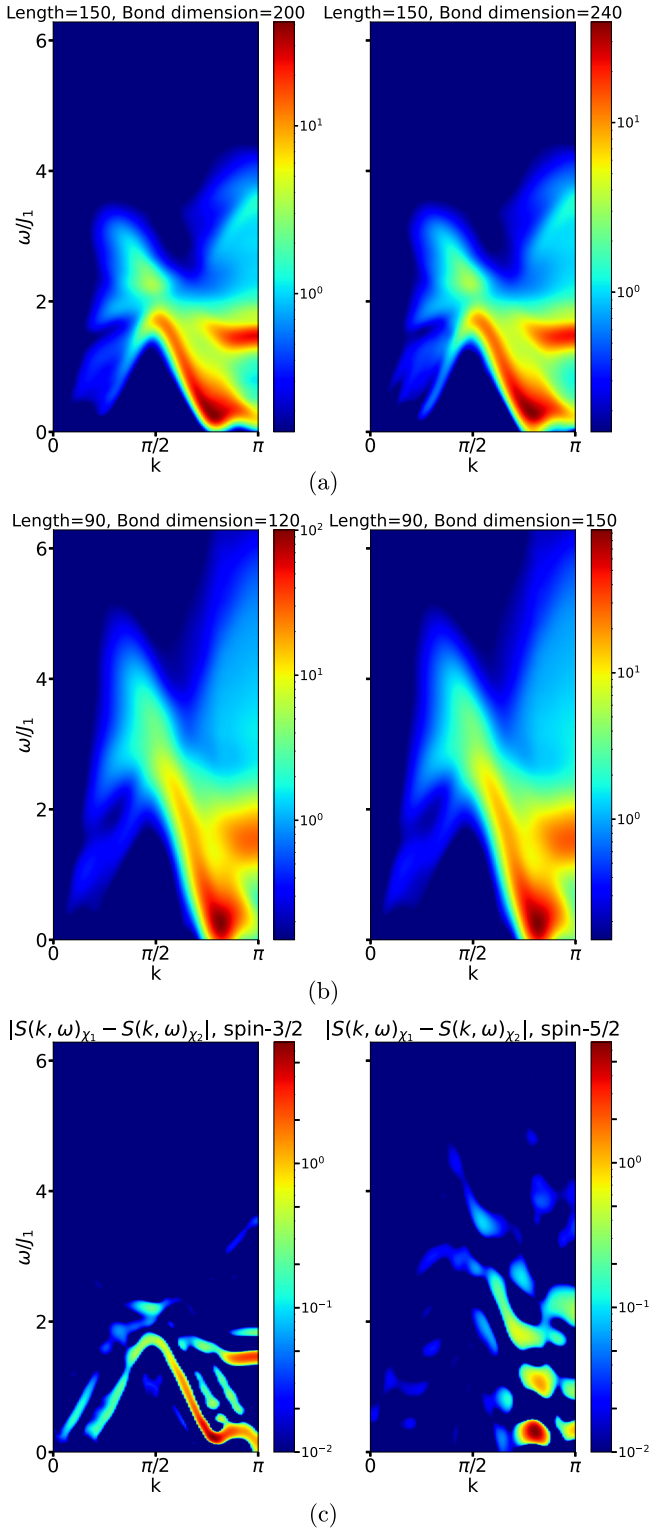

FIG. 10. (a) Spin-3/2 J_1-J_2 chain at $J_2 = 0.43J_1$, computed for a chain of length $L = 150$ with bond dimensions $\chi = 200$ and $\chi = 240$. (b) Spin-5/2 J_1-J_2 chain at $J_2 = 0.35J_1$, for a chain of length $L = 90$ with $\chi = 120$ and $\chi = 150$. In both cases, the DSF spectra remain qualitatively and quantitatively consistent, confirming that the chosen bond dimensions are sufficient to capture the essential features of the excitations. (c) Absolute difference $|S(k,\omega)_{\chi_1} - S(k,\omega)_{\chi_2}|$ between the two bond dimension results shown in panels (a) and (b), respectively.

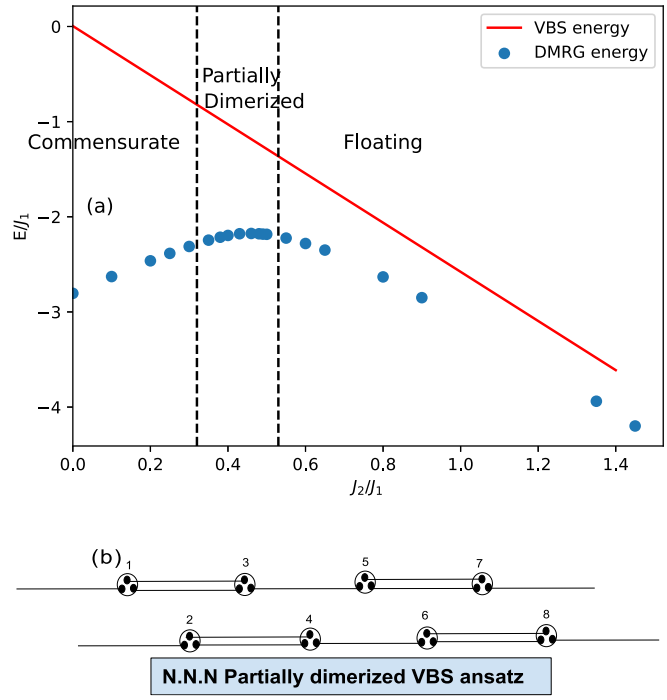

FIG. 11. (a) Comparison of variational energies per site from NNN-VBS *Ansatz* (red line), and DMRG results (blue dots) for the spin-3/2 J_1-J_2 chain. The NNN-VBS *Ansatz* matches the DMRG energies more closely in the floating phase ($J_2/J_1 \gtrsim 0.53$). (b) Cartoon of the next-nearest-neighbor (NNN) dimerized VBS *Ansatz* for the spin-3/2 J_1-J_2 chain. Black lines indicate NNN singlet bonds. Sites are shown as collections of three spin-1/2 particles symmetrized on site (black ovals). The illustrated configuration corresponds to an alternating pattern of one and two singlets per NNN bond.

APPENDIX B: CONVERGENCE WITH BOND DIMENSION IN DMRG CALCULATIONS

To verify the reliability of the DSF results presented in this work, we have examined the potential influence of the fixed bond dimension used during the ground-state optimization. While the dynamical correlation functions are computed using an MPS framework, the quality of the ground-state approximation is essential because it directly influences the computed spectral properties.

To rule out the possibility that the system is trapped in a metastable or locally suboptimal MPS due to an insufficient bond dimension, we have performed comparative calculations at two different system sizes and two corresponding bond dimensions for selected representative cases.

Specifically, for the spin-3/2 Heisenberg chain at $J_2 = 0.43$, we have carried out two independent sets of simulations: one at a system size of $L = 150$ with a fixed bond dimension $\chi = 200$, and another at $L = 150$ with a bond dimension $\chi = 240$ [Fig. 10(a)]. In both cases, the computed dynamical structure factors exhibit the same spectral features, with no qualitative or significant quantitative deviations observed. Similarly, for the spin-5/2 Heisenberg chain at $J_2 = 0.35$, we have performed calculations at $L = 90$ with $\chi = 120$, and at $L = 90$ with $\chi = 150$ [Fig. 10(b)]. Again, the spectra remain consistent across the two bond dimensions, confirming that

the observed features are not artifacts of a limited variational space but are genuine characteristics of the system.

To better visualize the effect of bond dimension on the computed DSF spectra, we also present in Fig. 10(c) the absolute difference between spectra obtained at two different bond dimensions: $|S(k,\omega)_{\chi_1} - S(k,\omega)_{\chi_2}|$, for both spin-3/2 and spin-5/2 chains. This difference plot directly quantifies the impact of varying χ and reveals that the changes are negligible.

These tests demonstrate that the fixed bond dimension employed throughout the ground-state calculations is sufficient for the parameter regimes studied here and does not compromise the physical reliability of the dynamical structure factor results presented in this work.

APPENDIX C: NEXT-NEAREST-NEIGHBOR DIMERIZED VBS *ANSATZ* IN THE FLOATING PHASE

In Sec. II C, we discussed that our partially dimerized valence bond solid (VBS) *Ansatz* is constructed with dimers located on nearest-neighbor (NN) bonds. This construction accurately reproduces the DMRG ground-state energy in the commensurate partially dimerized phase but deviates more strongly upon entering the floating phase. As pointed out in the main text, this discrepancy is due to the increasing importance of next-nearest-neighbor (NNN) singlet correlations at larger J_2/J_1.

To test this hypothesis, we constructed an alternative VBS *Ansatz* in which dimers are placed on NNN bonds in an alternating pattern of one and two singlets per bond (for $S = 3/2$). This pattern is shown schematically in Fig. 11(a), where the black lines represent NNN singlet bonds and the black dots indicate unpaired spin-1/2 constituents symmetrically combined on each site. The construction proceeds in the same spirit as the NN case: each spin-S site is decomposed into $2S$ spin-1/2 particles symmetrized on site, with valence bonds arranged to match the targeted dimerization pattern.

The resulting energies are plotted in Fig. 11(b) together with the DMRG results. As expected, the NNN-VBS *Ansatz* provides significantly lower variational energies in the floating phase ($J_2/J_1 \gtrsim 0.53$) and agrees more closely with DMRG data.

This analysis confirms that the increased discrepancy between the NN-VBS *Ansatz* and DMRG in the floating phase originates from the enhanced NNN singlet correlations, which are naturally captured by the modified NNN-VBS construction.

[1] T. Giamarchi, *Quantum Physics in One Dimension* (Oxford University Press, Oxford, UK, 2003), Vol. 121.

[2] I. Affleck, Quantum spin chains and the Haldane gap, J. Phys.: Condens. Matter **1**, 3047 (1989).

[3] F. D. M. Haldane, Continuum dynamics of the 1-D Heisenberg antiferromagnet: Identification with the O(3) nonlinear sigma model, Phys. Lett. A **93**, 464 (1983).

[4] C. K. Majumdar and D. K. Ghosh, On next-nearest-neighbor interaction in linear chain. I, J. Math. Phys. **10**, 1388 (1969).

[5] S. Eggert and I. Affleck, Numerical evidence for multiplicative logarithmic corrections from marginal operators, Phys. Rev. B **46**, 10866 (1992).

[6] A. Lavarélo and G. Roux, Spinon excitation spectra of the J_1-J_2 chain from analytical calculations in the dimer basis and exact diagonalization, Eur. Phys. J. B **87**, 1 (2014).

[7] F. Ferrari, A. Parola, S. Sorella, and F. Becca, Dynamical structure factor of the J_1-J_2 Heisenberg model in one dimension: The variational Monte Carlo approach, Phys. Rev. B **97**, 235103 (2018).

[8] S. R. White and I. Affleck, Dimerization and incommensurate spiral spin correlations in the zigzag spin chain: Analogies to the Kondo lattice, Phys. Rev. B **54**, 9862 (1996).

[9] K. Okamoto and K. Nomura, Fluid-dimer critical point in $S = 1/2$ antiferromagnetic Heisenberg chain with next nearest neighbor interactions, Phys. Lett. A **169**, 433 (1992).

[10] G. Müller, H. Thomas, H. Beck, and J. C. Bonner, Quantum spin dynamics of the antiferromagnetic linear chain in zero and nonzero magnetic field, Phys. Rev. B **24**, 1429 (1981).

[11] A. H. Bougourzi, M. Karbach, and G. Müller, Exact two-spinon dynamic structure factor of the one-dimensional Heisenberg model, Phys. Rev. B **57**, 11429 (1998).

[12] B. Lake, D. Tennant, C. Frost, and S. Nagler, Quantum criticality and universal scaling of a quantum antiferromagnet, Nat. Mater. **4**, 329 (2005).

[13] N. Chepiga, I. Affleck, and F. Mila, Dimerization transitions in spin-1 chains, Phys. Rev. B **93**, 241108(R) (2016).

[14] F. D. M. Haldane, Nonlinear field theory of large-spin Heisenberg antiferromagnets: Semiclassically quantized solitons of the one-dimensional easy-axis Néel state, Phys. Rev. Lett. **50**, 1153 (1983).

[15] I. Affleck, T. Kennedy, E. H. Lieb, and H. Tasaki, Rigorous results on valence-bond ground states in antiferromagnets, Phys. Rev. Lett. **59**, 799 (1987).

[16] G. Fath and J. Sólyom, Solitonic excitations in the Haldane phase of an $S = 1$ chain, J. Phys.: Condens. Matter **5**, 8983 (1993).

[17] A. Kolezhuk, R. Roth, and U. Schollwöck, First order transition in the frustrated antiferromagnetic Heisenberg $S = 1$ quantum spin chain, Phys. Rev. Lett. **77**, 5142 (1996).

[18] J. H. Pixley, A. Shashi, and A. H. Nevidomskyy, Frustration and multicriticality in the antiferromagnetic spin-1 chain, Phys. Rev. B **90**, 214426 (2014).

[19] A. Sharma, M. Nayak, H. M. Rønnow, and F. Mila, Bound states and deconfined spinons in the dynamical structure factor of the J_1-J_2 spin-1 chain, Phys. Rev. B **111**, 064404 (2025).

[20] L. Vanderstraeten, E. Wybo, N. Chepiga, F. Verstraete, and F. Mila, Spinon confinement and deconfinement in spin-1 chains, Phys. Rev. B **101**, 115138 (2020).

[21] N. Chepiga, I. Affleck, and F. Mila, Floating, critical, and dimerized phases in a frustrated spin-3/2 chain, Phys. Rev. B **101**, 174407 (2020).

[22] N. Chepiga, I. Affleck, and F. Mila, From $SU(2)_5$ to $SU(2)_3$ Wess-Zumino-Witten transitions in a frustrated spin-5/2 chain, Phys. Rev. B **105**, 174402 (2022).

[23] S. Rachel, Spin 3/2 dimer model, Europhys. Lett. **86**, 37005 (2009).

[24] R. Roth and U. Schollwöck, Frustrated antiferromagnetic quantum spin chains for spin length $S > 1$, Phys. Rev. B **58**, 9264 (1998).
[25] I. Affleck, T. Kennedy, E. H. Lieb, and H. Tasaki, Valence bond ground states in isotropic quantum antiferromagnets, Commun. Math. Phys. **115**, 477 (1988).
[26] H. Niggemann, A. Klümper, and J. Zittartz, Quantum phase transition in spin-3/2 Heisenberg antiferromagnetic chains: A valence bond solid study, Z. Phys. B: Condens. Matter **104**, 103 (1997).
[27] H.-H. Tu, G.-M. Zhang, and T. Xiang, Valence bond solid states with symplectic symmetry, J. Phys. A: Math. Theor. **41**, 415201 (2008).
[28] S. R. White and A. E. Feiguin, Real-time evolution using the density matrix renormalization group, Phys. Rev. Lett. **93**, 076401 (2004).
[29] S. R. White and I. Affleck, Spectral functions with the density matrix renormalization group: Krylov-space approach, Phys. Rev. B **77**, 134437 (2008).
[30] R. P. Feynman, Atomic theory of the two-fluid model of liquid helium, Phys. Rev. **94**, 262 (1954).
[31] A. Bijl, The lowest wave function of the symmetrical many particles system, Physica **7**, 869 (1940).
[32] D. P. Arovas, A. Auerbach, and F. D. H. Haldane, Extended Heisenberg models of antiferromagnetism: Analogies to the fractional quantum Hall effect, Phys. Rev. Lett. **60**, 531 (1988).
[33] A. Auerbach, *Interacting Electrons and Quantum Magnetism* (Springer, New York, 1998).
[34] U. Schollwöck, The density-matrix renormalization group in the age of matrix product states, Ann. Phys. (NY) **326**, 96 (2011).
[35] S. R. White, Density matrix formulation for quantum renormalization groups, Phys. Rev. Lett. **69**, 2863 (1992).
[36] S. R. White, Density-matrix algorithms for quantum renormalization groups, Phys. Rev. B **48**, 10345 (1993).
[37] U. Schollwöck, The density-matrix renormalization group, Rev. Mod. Phys. **77**, 259 (2005).
[38] G. Vidal, Efficient simulation of one-dimensional quantum many-body systems, Phys. Rev. Lett. **93**, 040502 (2004).
[39] A. J. Daley, C. Kollath, U. Schollwöck, and G. Vidal, Time-dependent density-matrix renormalization-group using adaptive effective Hilbert spaces, J. Stat. Mech. (2004) P04005.
[40] A. E. Feiguin and S. R. White, Time-step targeting methods for real-time dynamics using the DMRG, Phys. Rev. B **72**, 020404(R) (2005).
[41] S. M. Girvin, A. H. MacDonald, and P. M. Platzman, Magneto-roton theory of collective excitations in the fractional quantum Hall effect, Phys. Rev. B **33**, 2481 (1986).
[42] B. Lake, D. A. Tennant, J. S. Caux, T. Barthel, U. Schollwock, S. E. Nagler, and C. D. Frost, Multispinon continua at zero and finite temperature in a near-ideal Heisenberg chain, Phys. Rev. Lett. **111**, 137205 (2013).
[43] J. Des Cloizeaux and J. Pearson, Spin-wave spectrum of the antiferromagnetic linear chain, Phys. Rev. **128**, 2131 (1962).
[44] A. Deschner and E. S. Sørensen, Incommensurability effects in odd length J_1-J_2 quantum spin chains: On-site magnetization and entanglement, Phys. Rev. B **87**, 094415 (2013).
[45] N. Chepiga and F. Mila, Floating phase versus chiral transition in a 1D hard-boson model, Phys. Rev. Lett. **122**, 017205 (2019).
[46] K. Boya, K. Nam, A. K. Manna, J. Kang, C. Lyi, A. Jain, S. M. Yusuf, P. Khuntia, B. Sana, V. Kumar, A. V. Mahajan, D. R. Patil, K. H. Kim, S. K. Panda, and B. Koteswararao, Magnetic properties of the $s = 5/2$ anisotropic triangular chain compound $Bi_3FeMo_2O_{12}$, Phys. Rev. B **104**, 184402 (2021).
[47] L. Ornstein and F. Zernike, Die linearen dimensionen der dichteschwankungen, Phys. Zeit. **19**, 134 (1918).
[48] L. Ornstein and F. Zernike, Bemerkung zur arbeit von herrn kc kar: Die molekularzerstreuung des lichtes beim kritischen zustande, Phys. Zeit. **27**, 761 (1926).